INTERNATIONAL JOURNAL FOR NUMERICAL METHODS IN FLUIDS, VOL. 13, 759–773 (1991)

APPLICATION OF TAYLOR–LEAST SQUARES FINITE ELEMENT TO THREE-DIMENSIONAL ADVECTION–DIFFUSION EQUATION

N.-S. PARK

HydroGeoLogic, Inc., Herndon, VA, U.S.A.

AND

J. A. LIGGETT

School of Civil and Environmental Engineering, 273 Hollister Hall, Cornell University, Ithaca, NY, U.S.A.

SUMMARY

The Taylor–least squares (TLS) scheme, developed to solve the unsteady advection–diffusion equation for advection-dominated cases in one and two dimensions, is extended to three dimensions and applied to some 3D examples to demonstrate its accuracy. The serendipity Hermite element is selected as an interpolation function on a linear hexagonal element. As a validation of the code and as a simple sensitivity analysis of the scheme on the different types of shape functions, the 2D example problem of the previous study is solved again. Four 3D problems, two with advection and two with advection–diffusion, are also solved. The first two examples are advection of a steep 3D Gaussian hill in rotational flow fields. For the advection–diffusion problems with fairly general flow fields and diffusion tensors, analytical solutions are obtained using the ray method. Despite the steepness of the initial conditions, very good agreement is observed between the analytical and TLS solutions.

KEY WORDS Advection Diffusion Finite element Taylor–least squares

1. INTRODUCTION

The transport equation for a scalar quantity $c(\mathbf{x}, t)$ can be written as

$$\frac{\partial c}{\partial t} + \mathbf{u} \cdot \nabla c = \nabla \cdot (\mathbf{D} \cdot \nabla c), \tag{1}$$

where $\mathbf{u}(\mathbf{x}, t)$ is the velocity field of an incompressible flow, $\mathbf{D}(\mathbf{x})$ is the diffusion tensor and ∇ is the gradient operator in the global co-ordinate $\mathbf{x} = (x, y, z)$ which coincides with the principal axes of the symmetric diffusion tensor. With proper initial and boundary conditions, (1) constitutes a well-posed problem.

The Taylor–least squares (TLS) finite element scheme has been developed for advection-dominated problems.[1] The scheme in conjunction with Hermite elements has been tested rigorously and shown to be successful in one and two dimensions using the advection–diffusion equation. Unlike some other schemes developed for the same class of problems, the scheme does not require special treatment for one-, two- and three-dimensional problems nor for the shape of elements. Moreover, there are no arbitrary parameters to be optimized. It was also shown that the

0271–2091/91/160759–15$07.50

Received 26 March 1990
Revised 2 January 1991

Lax–Wendroff Taylor–Galerkin method of Donea *et al.*[2] and the Crank–Nicolson least squares scheme of Carey and Jiang[3] are special cases of the TLS scheme when linear elements are used. In this study the TLS scheme is applied to the three-dimensional advection–diffusion equation to demonstrate its straightforward application and its accuracy in example problems.

The derivation of the TLS equation for the advection-diffusion equation is given in Reference 1 and only a brief description will be given herein. The 3D serendipity Hermite elements,[4] specified on a hexahedron, are selected as a basis function. The Hermite elements, which have gradients in local co-ordinates, allow direct application of derivative boundary conditions without integrating by parts. The 3D formulation is tested against 2D and 3D problems. Since the examples in lower dimensions are the same reference problems that were solved by a different type of Hermite functions, one may see the sensitivity of the scheme on various types of shape functions. The results compare well with the previous results. In the absence of good 3D reference problems a few examples with interesting flow fields are generated.

2. THE TAYLOR–LEAST SQUARES FORMULATION

The formulation of the TLS equation for the advection–diffusion equation is given elsewhere[1] and will not be explained in detail herein. The following constitutes a brief summary.

2.1. The TLS method for the advection–diffusion equation

For any finite time interval $k = t^{n+1} - t^n$ an operator-splitting scheme can be used to decompose the advection–diffusion equation into two parts. For the advection part

$$\frac{\partial c_1}{\partial t} + \mathbf{u} \cdot \nabla c_1 = 0, \tag{2}$$

with $c_1(\mathbf{x}, nk) = c(\mathbf{x}, nk)$, and for the diffusion part

$$\frac{\partial c_2}{\partial t} = \nabla \cdot (\mathbf{D} \cdot \nabla c_2), \tag{3}$$

with $c_2(\mathbf{x}, nk) = c_1(\mathbf{x}, (n+1)k)$. Following the procedure given in Reference 1, the semidiscrete equation for the advection is obtained as

$$\{1 + [\alpha_1 \mathbf{u} + \alpha_2 (\mathbf{u} \cdot \nabla)\mathbf{u}] \cdot \nabla + \alpha_2 \mathbf{uu} : \nabla\nabla\} c_1^{n+1} = \{1 + [\beta_1 \mathbf{u} + \beta_2 (\mathbf{u} \cdot \nabla)\mathbf{u}] \cdot \nabla + \beta_2 \mathbf{uu} : \nabla\nabla\} c_1^n, \tag{4}$$

in which

$$\alpha_1 = \theta k, \qquad \beta_1 = -(1-\theta)k, \qquad \alpha_2 = -\frac{k^2}{2}\left(\frac{1}{3} - \theta\right), \qquad \beta_2 = \frac{k^2}{2}\left(\frac{2}{3} - \theta\right), \tag{5}$$

where $\theta \in [0, 1]$ is the time-weighting factor. For time-dependent flow $\mathbf{u}^{n+1}$ and $\mathbf{u}^n$ are used in (4) in an obvious manner. Note that the first two terms in braces represent the standard θ-weighted discretization of the advection equation and the last two terms are higher-order corrections. On the other hand, the temporal discretization for the 'well-behaved' diffusion part is approximated by the second-order Crank–Nicolson scheme

$$\frac{c_2^{n+1} - c_2^n}{k} = \tfrac{1}{2}[\nabla \cdot (\mathbf{D} \cdot \nabla)](c_2^{n+1} + c_2^n). \tag{6}$$

The two semidiscrete equations (4) and (6) are added before spatial discretization by the least squares scheme is performed. The intermediate variables in the resulting equation are removed by the definitions of the initial conditions and Taylor series expansions. The semidiscrete equation

for the advection–diffusion equation becomes

$$\mathscr{A}_1 c^{n+1} = \mathscr{A}_2 c^n, \tag{7}$$

where

$$\mathscr{A}_1 = 1 + \alpha_1 \mathbf{u}\cdot\nabla + \alpha_2[(\mathbf{u}\cdot\nabla)\mathbf{u}]\cdot\nabla + \alpha_2 \mathbf{u}\mathbf{u}:\nabla\nabla - \frac{k}{2}[\nabla\cdot(\mathbf{D}\cdot\nabla)],$$

$$\mathscr{A}_2 = 1 + \beta_1 \mathbf{u}\cdot\nabla + \beta_2[(\mathbf{u}\cdot\nabla)\mathbf{u}]\cdot\nabla + \beta_2 \mathbf{u}\mathbf{u}:\nabla\nabla + \frac{k}{2}[\nabla\cdot(\mathbf{D}\cdot\nabla)].$$

By using the operator-splitting scheme, one avoids the use of prohibitively higher-order shape functions which would have been required if the TLS scheme were applied directly to the advection–diffusion equation. The primary disadvantage of the operator-splitting scheme, related to the violation of a downstream boundary condition during advection steps, is also circumvented by adding the two semidiscrete equations and solving the resulting equations using the least squares procedure. Fully discrete TLS equations for the advection–diffusion equation are obtained by equating the variation of the least squares functional for (7) to zero:

$$\int_\Omega d\Omega(\mathscr{A}_1 c^{n+1} - \mathscr{A}_2 c^n).\mathscr{A}_1 \delta c^{n+1} = 0. \tag{8}$$

Identifying δc^{n+1} as a weighting function, the above equation yields a system of algebraic equation when applied to elements.

At this stage the usual practice of the popular Galerkin finite element method is to integrate (8) by parts. The purpose is twofold: (i) to reduce the order of the highest derivative in the integrand so that lower-order interpolation functions can be used; (ii) to derive boundary integrals involving flux terms so that derivative boundary conditions can be applied. With the least squares finite element method one cannot hope to reduce the order of derivatives in the integrand through integration by parts, since equal-order derivatives are already present in the weighting function. Therefore, if integration by parts were used to derive boundary integral terms, the order of the highest derivative in the integrand would have been increased by one. However, one does not have to face that penalty to apply boundary conditions involving derivatives in this case. Since Hermite functions are used, derivative boundary conditions can be applied explicitly by specifying proper derivative unknowns in the interpolation function. Most derivative boundary conditions are given in terms of normal flux and it is trivial to specify normal fluxes on a boundary because the derivative unknowns are in local co-ordinates. On Dirichlet boundaries, not only nodal unknowns of the function but also its tangential derivatives must be specified at the corresponding boundary nodes to have a unique function.

3. SERENDIPITY HERMITE ELEMENT

A complete Hermite interpolation function for an eight-node hexahedron involves 10 degrees of freedom per node.[4] Since the additional accuracy obtained by using the complete Hermite element instead of a serendipity element, which has four degrees of freedom, hardly compensates the increase in computational expense, the serendipity Hermite element proposed in Reference 4 (p. 143) is used. A hexahedron in global and local co-ordinates is given in Figure 1. Using repeated indices to indicate summation, the element can be written as

$$c(\mathbf{r}, t) = c_j(t) N_j(\mathbf{r}) + \frac{\partial c_j}{\partial r_p}(t) M_{pj}(\mathbf{r}), \qquad p = 1, 3, \quad j = 1, 8, \tag{9}$$

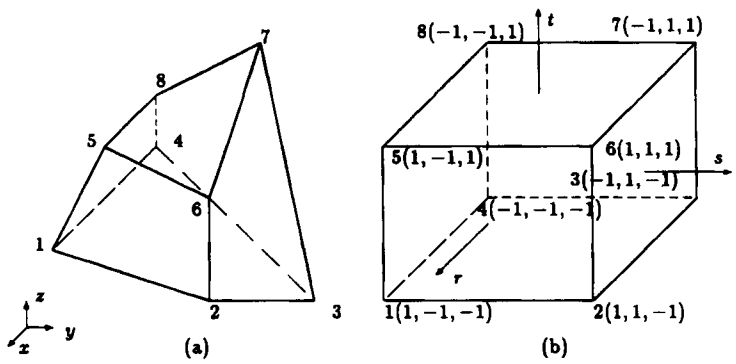

Figure 1. Hexahedral elements in (a) global and (b) local co-ordinates

where c_j is the nodal unknown, $\partial c_j/\partial r_s$ are components of the gradient in local co-ordinates and N_i and M_{ij} are shape functions in which $\mathbf{r}=(p, q, r)$ is a local co-ordinate vector. Note that the gradient in (9) is with respect to the local co-ordinate $\mathbf{r}$. The basis functions are defined as follows:

$$N_j(\mathbf{r})=\frac{\phi_j}{2}(2+p_0p+q_0q+r_0r-p^2-q^2-r^2),$$

$$M_{1j}(\mathbf{r})=-\frac{r_0}{2}\phi_j(1-p^2), \qquad M_{2j}(\mathbf{r})=-\frac{s_0}{2}\phi_j(1-q^2), \qquad M_{3j}(\mathbf{r})=-\frac{t_0}{2}\phi_j(1-r^2),$$

where the usual Lagrange trilinear basis function for a cube is

$$\phi_j(\mathbf{r})=\tfrac{1}{8}(1+p_0p)(1+q_0q)(1+r_0r),$$

in which (r_0, s_0, t_0) is the local co-ordinate of the local node j (Figure 1).

The specification of the basis function completes the derivation of the three-dimensional TLS scheme. However, the TLS formula in (8) is given in global co-ordinates and the basis function in (9) is given in local co-ordinates. To evaluate the integrations, it is necessary to transform the derivatives into local co-ordinates:

$$\frac{\partial c}{\partial r_p}=\frac{\partial x_k}{\partial r_p}\frac{\partial c}{\partial x_k}, \tag{10}$$

or in a matrix notation

$$\nabla_r c=\mathbf{J}\nabla_x c, \tag{11}$$

where a subscript is used to indicate the co-ordinates in which the gradient is evaluated and $\mathbf{J}$ is the Jacobian matrix. The transformation of the gradient from the local to the global co-ordinates becomes

$$\nabla_x c=\mathbf{J}^{-1}\nabla_r c. \tag{12}$$

The transformation of the artificial diffusion tensor $\nabla\nabla$ in (7) is more subtle. Using the chain rule of differentiation, the second derivative in local co-ordinates can be written in global derivatives:

$$\frac{\partial^2}{\partial r_i\partial r_j}=\frac{\partial^2 x_p}{\partial r_i\partial r_j}\frac{\partial}{\partial x_p}+\frac{\partial x_p}{\partial r_i}\frac{\partial x_m}{\partial r_j}\frac{\partial^2}{\partial x_p\partial x_m}. \tag{13}$$

Inversion of the fourth-order tensor on the right-hand side of (13) poses computational difficulty. However, one can convert the fourth-order tensor into a second-order tensor by writing the independent part of the diffusion matrix as a vector. To that end, (13) is rewritten as

$$\Delta_r = \mathbf{H}\nabla_x + \mathbf{K}\Delta_x, \tag{14}$$

where

$$\Delta_r = \left[\frac{\partial^2}{\partial p^2}\ \frac{\partial^2}{\partial p\partial q}\ \frac{\partial^2}{\partial p\partial r}\ \frac{\partial^2}{\partial q^2}\ \frac{\partial^2}{\partial q\partial r}\ \frac{\partial^2}{\partial r^2}\right]^{\mathrm{T}},$$

$$\Delta_x = \left[\frac{\partial^2}{\partial x^2}\ \frac{\partial^2}{\partial x\partial y}\ \frac{\partial^2}{\partial x\partial z}\ \frac{\partial^2}{\partial y^2}\ \frac{\partial^2}{\partial y\partial z}\ \frac{\partial^2}{\partial z^2}\right]^{\mathrm{T}},$$

$$\mathbf{H} = \begin{bmatrix} 0 & x_{,pq} & x_{,pr} & 0 & x_{,qr} & 0 \\ 0 & y_{,pq} & y_{,pr} & 0 & y_{,qr} & 0 \\ 0 & z_{,pq} & z_{,pr} & 0 & z_{,qr} & 0 \end{bmatrix}^{\mathrm{T}},$$

$$\mathbf{K} = \begin{bmatrix} (x_{,p})^2 & 2x_{,p}y_{,p} & 2x_{,p}z_{,p} & (y_{,p})^2 & 2y_{,p}z_{,p} & (z_{,p})^2 \\ x_{,p}x_{,q} & x_{,p}y_{,q}+y_{,p}x_{,q} & 2x_{,p}z_{,q}+z_{,p}x_{,q} & y_{,p}y_{,q} & y_{,p}z_{,q}+z_{,p}y_{,q} & z_{,p}z_{,q} \\ x_{,p}x_{,r} & x_{,p}y_{,r}+y_{,p}x_{,r} & 2x_{,p}z_{,r}+z_{,p}x_{,r} & y_{,p}y_{,r} & y_{,p}z_{,r}+z_{,p}y_{,r} & z_{,p}z_{,r} \\ (x_{,q})^2 & 2x_{,q}y_{,q} & 2x_{,q}z_{,q} & (y_{,q})^2 & 2y_{,q}z_{,q} & (z_{,q})^2 \\ x_{,q}x_{,r} & x_{,q}y_{,r}+y_{,q}x_{,r} & 2x_{,q}z_{,r}+z_{,q}x_{,r} & y_{,q}y_{,r} & y_{,q}z_{,r}+z_{,q}y_{,r} & z_{,q}z_{,r} \\ (x_{,r})^2 & 2x_{,r}y_{,r} & 2x_{,r}z_{,r} & (y_{,r})^2 & 2y_{,r}z_{,r} & (z_{,r})^2 \end{bmatrix}.$$

Note that the zeros in the **H**-matrix are due to the trilinearity of the element geometry and that the **K**-matrix is readily available once the Jacobian is computed. Finally, the second derivatives are expressed in terms of local co-ordinates

$$\Delta_x = \mathbf{K}^{-1}(\Delta_r - \mathbf{H}\nabla_x) = \mathbf{K}^{-1}(\Delta_r - \mathbf{H}\mathbf{J}^{-1}\nabla_r) \tag{15}$$

using (12). Substituting (12) and (15) into (8), one obtains

$$\int_{-1}^{1}\int_{-1}^{1}\int_{-1}^{1} \mathrm{d}p\,\mathrm{d}q\,\mathrm{d}r\,\det(\mathbf{J})(\mathscr{A}_1 c^{n+1} - \mathscr{A}_2 c^n)\mathscr{A}_1\,\delta c^{n+1} = 0, \tag{16}$$

where $\mathscr{A}_1$ and $\mathscr{A}_2$ are now written in terms of local co-ordinate **r**. The integrals can be evaluated by an appropriate numerical integration scheme, for example

$$\int_{-1}^{1}\int_{-1}^{1}\int_{-1}^{1} f(p,q,r)\,\mathrm{d}p\,\mathrm{d}q\,\mathrm{d}r = \sum_{k=1}^{n}\sum_{j=1}^{n}\sum_{i=1}^{n} w_i w_j w_k f(p_i, q_j, r_k), \tag{17}$$

where n is the number of sampling points, (p_i, q_i, r_i) is a sampling point and w_i is the weight associated with the sampling point.

4. NUMERICAL EXAMPLES

In this section the 3D TLS finite element scheme is tested against some example problems. First, the scheme is applied to one- and two-dimensional standard reference problems[5] to validate the code and to examine the sensitivity of the different shape functions on the TLS scheme. Then, fully three-dimensional example problems are used to test the algorithm. Unfortunately, the authors

cannot find standard 3D example problems equivalent to those analysed in lower dimensions. Four 3D problems, with or without diffusion, are generated. Some parameters, especially initial conditions, flow velocities and diffusion coefficients, are determined such that the 3D advection–diffusion equation can be solved analytically using the ray method.[6-8]

4.1. Lower-dimensional examples

The one-dimensional standard problems are advection of a sharp front and of a steep Gaussian hill and have been solved accurately using the two-dimensional TLS scheme in our previous study.[1] For the one-dimensional problems the 3D seredipity Hermite element reduces identically to the one-dimensional element used previously and the results are not reported herein.

The two-dimensional example involves a Gaussian hill in a rotating flow field. In the previous study a special non-conforming Hermite triangular element[9] was used. Since the 3D serendipity element does not reduce to the 2D element when the dependence on the third direction vanishes, the result is reported herein as a simple sensitivity analysis of the TLS scheme on the different types of elements. The domain used in the 2D example is

$$x,\ y \in [-3200, 3200], \qquad z \in [-100, 100].$$

Note that an arbitrary thickness in the z-direction has been added to the two dimensional domain so that the 3D TLS code can be used. The domain is discretized by 1024 subcubes each of size $200 \times 200 \times 200$. The rotational flow field is given by

$$\mathbf{u} = \Omega(-y, x, 0)^{\mathrm{T}}, \tag{18}$$

where $\Omega = \pi/1000$. The initial condition is specified by

$$c(\mathbf{x}, 0) = \exp\left(-\frac{x^2 + (y+1600)^2}{2\sigma^2}\right), \tag{19}$$

where $\sigma = 264$ and the boundary condition is

$$c(\Gamma, t) = 0, \tag{20}$$

where Γ is the inflow boundary.

A time step of 10 is used and the solution is examined after a full rotation. The solutions at $z = -100$ and 100 are given in Figure 2. The two results are almost identical, showing no grid orientation effects. After one revolution the peak has been reduced to 0·95, indicating additional dissipation compared to that of the two-dimensional TLS which resulted in dissipation at the peak of about 2%. Nevertheless, the preservation of the symmetry of the hill is very good and the hill is still contained within four elements in either the x- or y-direction as in the initial condition.

4.2. Three-dimensional examples

The ray method was originally developed[6] and extended[7,8] for high-Peclet-number point source problems in an unbounded domain. The method uses an asymptotic technique and solutions are generally in the form of infinite series. However, in some limiting cases the ray method yields closed-form solutions, i.e. the asymptotic solution terminates within a finite number of terms; in fact, only one term. In this study the flow field and the diffusion coefficients are selected such that exact analytical solutions can be obtained. The flow field used in this study consists of two components: linear shear and uniform translation, i.e.

$$\mathbf{u}(\mathbf{x}) = \boldsymbol{\Omega}\mathbf{x} + \mathbf{v}, \tag{21}$$

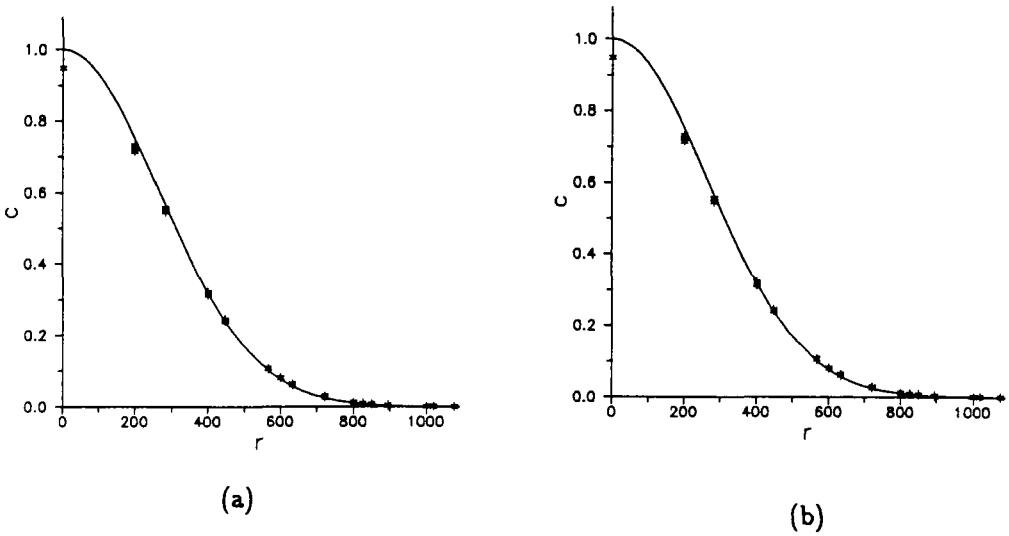

Figure 2. TLS result for the 2D example (a) at $z=100$ and (b) at $z=-100$: ——, analytical; *, TLS

where $\mathbf{v}=(v_x, v_y, v_z)^{\mathrm{T}}$ is a constant vector representing the uniform flow component and the constant shear matrix $\boldsymbol{\Omega}$ is

$$\boldsymbol{\Omega}=\begin{bmatrix} 0 & \omega_{12} & 0 \\ \omega_{21} & 0 & \omega_{23} \\ 0 & \omega_{32} & 0 \end{bmatrix}.$$

The non-zero eigenvalues of $\boldsymbol{\Omega}$ are

$$\mu=\pm\sqrt{(\omega_{12}\omega_{21}-\omega_{23}\omega_{32})}. \tag{22}$$

Depending on the sign of the term under the square root, qualitatively different flow patterns are obtained. When the eigenvalues are real, trajectories of flow particles are in the form of hyperbolas; and when imaginary, they take on the form of ellipses. The diffusion coefficients used in this study are

$$\mathbf{D}=\begin{bmatrix} D_{xx} & 0 & 0 \\ 0 & D_{yy} & 0 \\ 0 & 0 & D_{zz} \end{bmatrix}, \tag{23}$$

in which elements are assumed to be constant. In the following examples different combinations of (21) and (23) are used. The ray method yields exact analytical solutions for far more general forms of $\boldsymbol{\Omega}$ and $\mathbf{D}$ than those used in this study.

The flow field given by (21) can be integrated to yield the expression for the trajectory of a fluid particle initially at $\mathbf{x}^0$:

$$\mathbf{x}(t)=\alpha t\begin{Bmatrix} \omega_{23} \\ 0 \\ -\omega_{21} \end{Bmatrix}+\begin{Bmatrix} \omega_{12}\left(\beta\dfrac{e^{\mu t}+e^{-\mu t}}{2}+\gamma\dfrac{e^{\mu t}-e^{-\mu t}}{2\mu}\right) \\ \gamma\dfrac{e^{\mu t}+e^{-\mu t}}{2}+\beta\mu^2\dfrac{e^{\mu t}-e^{-\mu t}}{2\mu} \\ \omega_{32}\left(\beta\dfrac{e^{\mu t}+e^{-\mu t}}{2}+\gamma\dfrac{e^{\mu t}-e^{-\mu t}}{2\mu}\right) \end{Bmatrix}+\begin{Bmatrix} x^0-\omega_{12}\beta \\ y^0-\gamma \\ z^0-\omega_{32}\beta \end{Bmatrix}, \tag{24}$$

where

$$\alpha=\frac{\omega_{32}v_x-\omega_{12}v_x}{\mu^2},\qquad \beta=\frac{\omega_{21}x^0+\omega_{23}z^0+v_y}{\mu^2},\qquad \gamma=y^0+\frac{\omega_{23}v_z+\omega_{21}v_x}{\mu^2}.$$

When μ is imaginary, the flow field becomes rotational with an angular velocity of $\hat{\mu}$ ($=|\mu|$). Then (24) reduces at $t=2\pi/\hat{\mu}$ to the following:

$$\mathbf{x}\left(\frac{2\pi}{\hat{\mu}}\right)=\begin{Bmatrix} x_0+\dfrac{\omega_{32}v_x-\omega_{12}v_z}{\mu^2}\omega_{23}\dfrac{2\pi}{\hat{\mu}} \\ y_0 \\ z_0-\dfrac{\omega_{32}v_x-\omega_{12}v_z}{\mu^2}\omega_{21}\dfrac{2\pi}{\hat{\mu}} \end{Bmatrix}. \tag{25}$$

Therefore, when $v_x=v_z=0$, the flow field becomes periodic regardless of the value of v_y. The effect of v_y is to move the centre of the rotation within the plane of rotation.

The analytical solution based on the ray method to the N-dimensional advection–diffusion equation for the given flow field and the diffusion coefficient is

$$c(\mathbf{x}, t)=A(t)\mathrm{e}^{-\Psi(\mathbf{x}, t)}, \tag{26}$$

where

$$A(t)=\frac{1}{(4\pi)^{N/2}}\left(\frac{\det\mathbf{M}(0)\det\mathbf{M}(t)}{\det\mathbf{S}(t)}\right)^{1/2},$$

$$\Psi(\mathbf{x}, t)=\frac{1}{4}\left(\mathbf{M}^{\mathrm{T}}\mathbf{x}-\int_0^t\mathbf{M}^{\mathrm{T}}\mathbf{v}\,\mathrm{d}\tau\right)^{\mathrm{T}}\mathbf{S}^{-1}\left(\mathbf{M}^{\mathrm{T}}\mathbf{x}-\int_0^t\mathbf{M}^{\mathrm{T}}\mathbf{v}\,\mathrm{d}\tau\right),$$

$$\mathbf{S}(t)=\int_0^t\mathbf{M}^{\mathrm{T}}\mathbf{D}\mathbf{M}\,\mathrm{d}\tau,$$

in which $\mathbf{M}(t)$ is any fundamental matrix solution of

$$\frac{\mathrm{d}\mathbf{M}}{\mathrm{d}t}=-\mathbf{\Omega}^{\mathrm{T}}\mathbf{M}. \tag{27}$$

For $\mathbf{\Omega}$ used in this study the fundamental matrix solution $\mathbf{M}$ becomes

$$\mathbf{M}(t)=\frac{1}{\mu^2}\left(\frac{\mathrm{e}^{\mu t}+\mathrm{e}^{-\mu t}}{2}-1\right)\mathbf{\Omega}^{\mathrm{T}}\mathbf{\Omega}^{\mathrm{T}}-\frac{\mathrm{e}^{\mu t}-\mathrm{e}^{-\mu t}}{2\mu}\mathbf{\Omega}^{\mathrm{T}}+\mathbf{I}, \tag{28}$$

where $\mathbf{I}$ is an identity matrix.

In the remainder of this section, four 3D example problems are presented along with analytical solutions. Two of them are pure advection and the other two are advection–diffusion. All examples share the same domain and spatial discretization. The domain is a cube of

$$x_i\in[-2400, 2400],\quad i=1, 2, 3,$$

and is discretized by 24^3 subcubes of a size $200\times200\times200$.

4.2.1. Pure advection case 1. The first 3D example is similar to the previous 2D example in that a 3D Gaussian hill is placed in a 3D rotational flow field. The initial condition is

$$c(x, 0)=\exp\left(-\frac{|\mathbf{x}-\mathbf{x}^0|^2}{2\sigma^2}\right), \tag{29}$$

where the centre of the hill is initially at $\mathbf{x}^0=(0, 0, -1000)$ and $\sigma=264$. The velocity field is specified by the shear matrix

$$\mathbf{\Omega}=\frac{\sqrt{2\pi}}{2000}\begin{bmatrix} 0 & 1 & 0 \\ -1 & 0 & 1 \\ 0 & -1 & 0 \end{bmatrix} \tag{30}$$

and the uniform flow component

$$\mathbf{v}=(0{\cdot}5, 0, 0{\cdot}5)^{\mathrm{T}}. \tag{31}$$

Boundary conditions

$$c(\Gamma, t)=0 \tag{32}$$

are used, where Γ is the inflow boundary.

The centre of the hill, initially at (0, 0, −1000), moves to (1000, 0, 0) at $t=2000$. The spiral-like trajectory of the centre of the hill from $t=0$ to 2000 is given in Figure 3(a). The Gaussian hill should remain identical to its initial shape after one revolution since there is no diffusion and the flow field has zero rate of strain e_{ij}, where

$$2e_{ij}=\frac{\partial u_i}{\partial x_j}+\frac{\partial u_j}{\partial x_i}. \tag{33}$$

A total of 200 uniform time steps are used to discretize one period for the TLS scheme. The resulting Gaussian hill is spherically symmetrical and the TLS result along with the analytical solution are reported in Figure 4. Note that the Gaussian hill is plotted with respect to the radial distance. The dissipation at the peak is about 10%. Considering the severity of the initial condition (the Gaussian hill reduces from 1 to 0·01 in four elements in all directions), the result is very good. Moreover, the spherical symmetry is well preserved as can be seen in the figure.

The resulting matrix equations (16) are solved by the Orthomin Accelerated Conjugate Gradient Solver developed by Sudicky on an IBM 3090 computer using its vector facility. No attempt was made to optimize the code; however, CPU times were 1380 s for the four-point Gaussian elemental integrations, 1800 s for the incomplete LU decomposition and 30 s for the back-substitution at each time step when the code was run in single precision. Note that, owing to the steadiness of the flow and the constant time step size, the numerical integrations and the decomposition are performed only once.

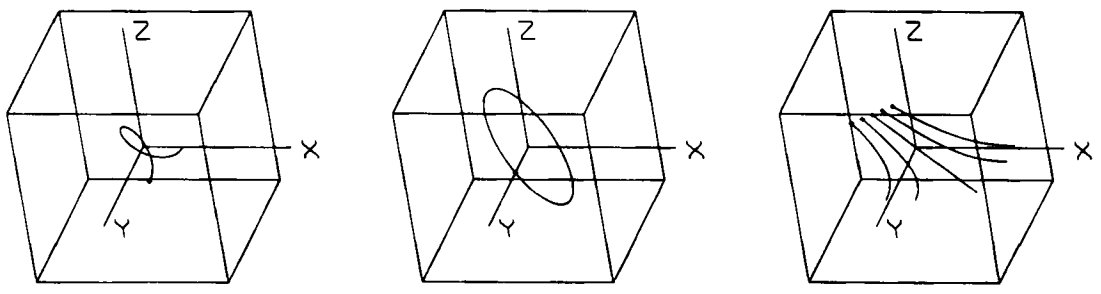

(a) (b) (c)

Figure 3. Trajectories of fluid particles for the example problems: (a) first advection case; (b) second advection case; (c) second advection–diffusion case; +, starting position

4.2.2. Pure advection case 2. This example, also pure advection of a 3D Gaussian hill, uses the same Gaussian hill as was used in the first example. The initial condition centres at (0, −1200, 0). The major difference from the first example is in the flow field. The shear matrix is given by

$$\mathbf{\Omega}=\frac{\pi}{2000\sqrt{2}}\begin{bmatrix}0 & 1 & 0\\ 1 & 0 & 3\\ 0 & -3 & 0\end{bmatrix} \tag{34}$$

and a zero uniform flow component is used. Unlike the first case, the rate of strain for this flow field is not zero; thus the hill will undergo deformation due to the flow field. The trajectory of the centre of the hill, specified by (24), is plotted in Figure 3(b). The flow field is periodic owing to the imaginary eigenvalues and the zero uniform flow component. Therefore the deformation during the first half of the rotation is exactly opposite that of the second half, so that any distortion of the hill is restored to the initial shape. The same boundary condition $c=0$ is used at inflow nodes. Again 200 time steps are used to complete one revolution of the hill. The result is given in Figure 5. After one revolution the peak has been reduced by about 14%. The decrease in accuracy as compared to the result of the first example is probably due to the non-zero rate of strain.

4.2.3. Advection–diffusion case 1. The first example with diffusion uses the same flow field as the first advection example. An isotropic diffusion tensor is selected and is given by

$$\mathbf{D}=5\mathbf{I}, \tag{35}$$

where $\mathbf{I}$ is the unity matrix. In addition to the usual $c=0$ inflow boundary condition, a condition of zero normal flux is used at the outflow boundary, i.e.

$$\nabla c\cdot\mathbf{n}=0, \tag{36}$$

where $\mathbf{n}$ is an outward normal vector.

The ray method gives analytical solutions for point source problems. To obtain an analytical solution for the example using the ray method, the initial condition also has to be determined

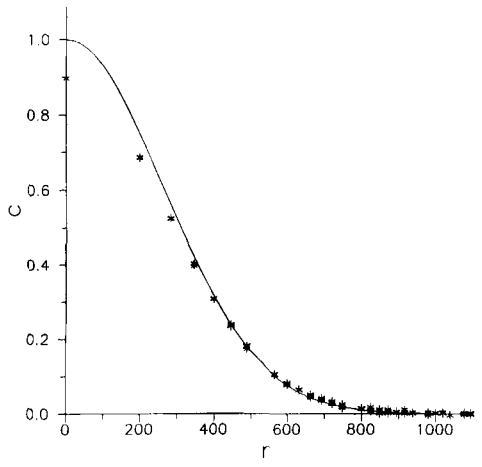

Figure 4. Result of first advection example: ——, analytical; *, TLS

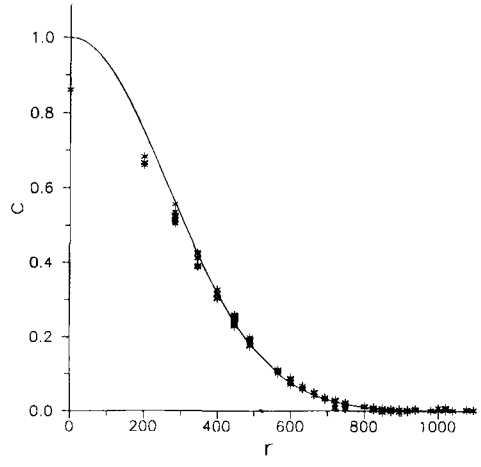

Figure 5. result of second advection example: ——, analytical; *, TLS

using the same method. The ray method assumes that the point source is initially at the origin. However, according to the flow field, the origin is on the centre of the rotation. An appropriate uniform y-velocity of $\sqrt{(2)}\pi/2$ is added to the uniform flow field (31) to move the centre of the rotation off the origin. The initial condition for the TLS scheme is obtained when the point source is diffused enough so that the resulting Gaussian hill can be resolved by the specified grid system. As in the advection problems, the initial condition is set so that the reduction of the peak value is 99% within four elements in any direction. At $t=4000$, or after two rotations, the point source has been diffused to a Gaussian hill of the desired steepness. The hill is subsequently normalized by its peak value to be used as the initial condition (Figure 6). For the TLS scheme the centre of the hill is placed at $(0, 0, -1000)$ to provide the same relative velocity field with respect to the hill. At $t=0$ the grid Peclet number, in the x-direction for example, at the centre is about 90, indicating that the transport is advection-dominated. A time step of 10 is used for the TLS scheme. The comparison between the TLS result after one revolution and the solution from the ray method at $t=6000$ is given in Figure 7. The ray method has a peak value of 0·54 and the peak of the TLS result is 0·50. The dissipation at the peak is about 8% and, as expected, is less than those of the advection examples. The spherical symmetry of the TLS result is also very good.

4.2.4. Advection–diffusion case 2. The second advection–diffusion example uses 2D flow with a stagnation point. The shear matrix is specified by

$$\mathbf{\Omega}=\begin{bmatrix}0 & \rho & 0\\ \rho & 0 & \varepsilon\\ 0 & \varepsilon & 0\end{bmatrix}, \tag{37}$$

in which $\rho=0{\cdot}006$ and $\varepsilon=10^{-20}$. ε is added to the $\mathbf{\Omega}$-matrix to allow (26) to have a solution. The non-zero eigenvalues for the shear matrix are real-valued and, consequently, the flow trajectories are hyperbolas with a stagnation point. The uniform flow components are

$$\mathbf{v}=\rho s(1, -1, 0)^{\mathrm{T}}, \tag{38}$$

where $s=2400$ and is determined such that the stagnation point is located at $(s, -s, 0)$. A simple 2D flow is used in this example to help visualize the flow field and to predict the effects on the

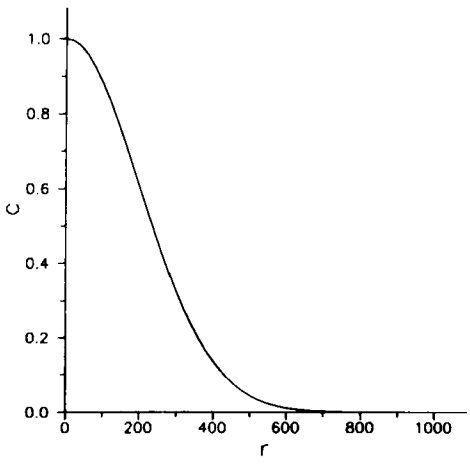

Figure 6. Initial condition for first advection–diffusion example

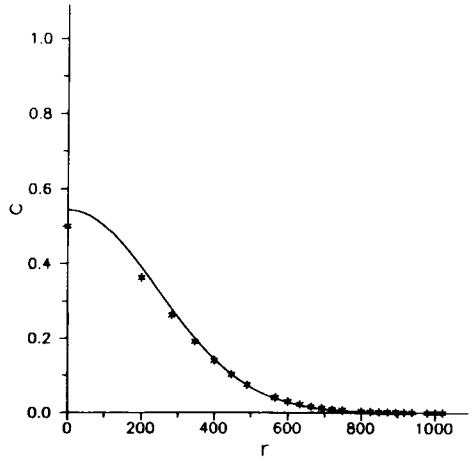

Figure 7. Result of first advection–diffusion example: ——, analytical; *, TLS

initial condition. Some trajectories of fluid particles are given in Figure 3(c). Although the flow field is two-dimensional, anisotropic diffusion coefficients are used to make the problem fully three-dimensional. The diffusion coefficients are

$$\mathbf{D}=\begin{bmatrix}150 & 0 & 0\\ 0 & 150 & 0\\ 0 & 0 & 200\end{bmatrix}. \tag{39}$$

The ray method is used to obtain an appropriate initial condition by advecting and diffusing a point source until the cloud is spread sufficiently. The normalized ray method result at $t=67{\cdot}5775$ is selected as an initial condition (Figure 8) and the centre of the hill is located at $(-800, 800, 0)$

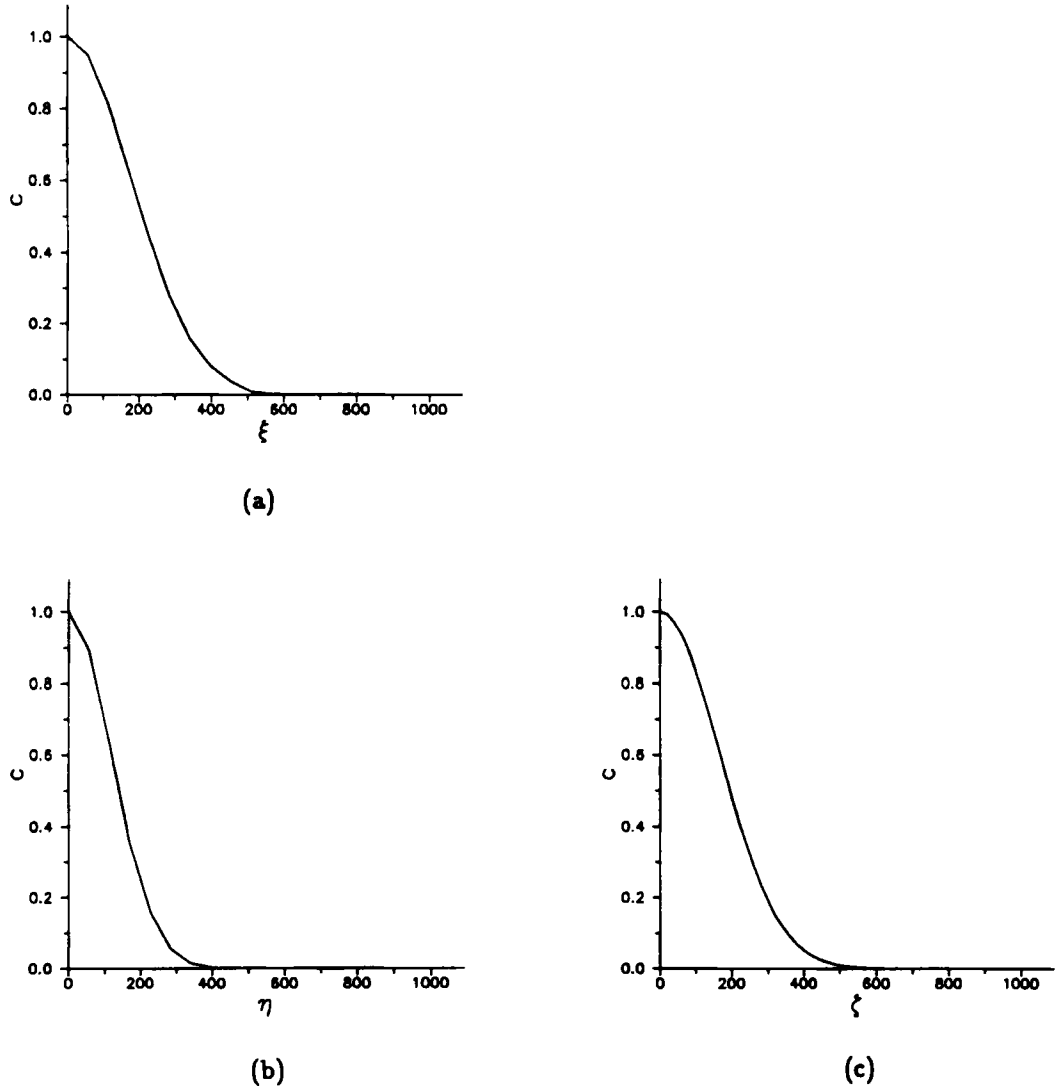

Figure 8. Initial condition for second advection–diffusion example in local co-ordinates (a) ξ, (b) η and (c) ζ

for the TLS. The shape of the initial condition, no longer spherically symmetric, is plotted in local co-ordinates ξ, η and ζ. The origin of the local co-ordinate system is at the centre of the hill and the local co-ordinates ξ and η are defined in the cross-sectional contour plot of the initial condition in Figure 9. The cross-section is in the plane $z=0$. The ζ-co-ordinate is parallel to the z-axis. The initial condition, especially in the η-direction, is extremely steep: the hill decreases to less than 1% of its peak in just two elements.

The ray method result at $t=183{\cdot}1025$ is selected as a final solution and the TLS scheme is applied using the initial condition for the duration of 115·525. Twenty uniform time steps are used to discretize the simulation time. After the simulation the centre of the hill is located at (800, −800, 0). For the given parameters the Peclet number at the centre of the hill is maximum at the starting time. The Peclet number in the x-direction varies from 25·6 at $t=0$ to 12·8 at $t=115$, which shows more pronounced effects of the diffusion than the first advection–diffusion example, but the problem is still advection-dominated.

The simulation result along with the analytical solution are plotted in local co-ordinates and reported in Figure 10. The peak value of the analytical solution is 0·19 while that of the TLS is 0·205. Unlike any of the previous examples an overshoot of 0·015 is observed. The cross-sectional contour plot of the analytical solution in the $z=0$ plane is also given in Figure 9.

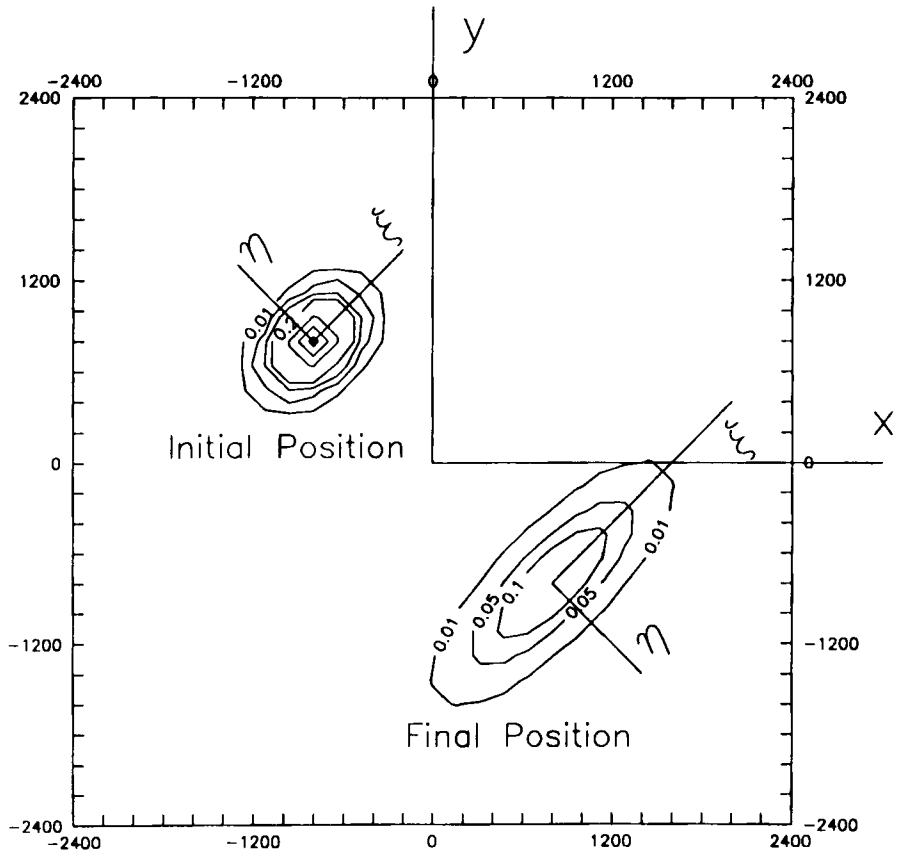

Figure 9. Definition of local co-ordinates used in second advection–diffusion example

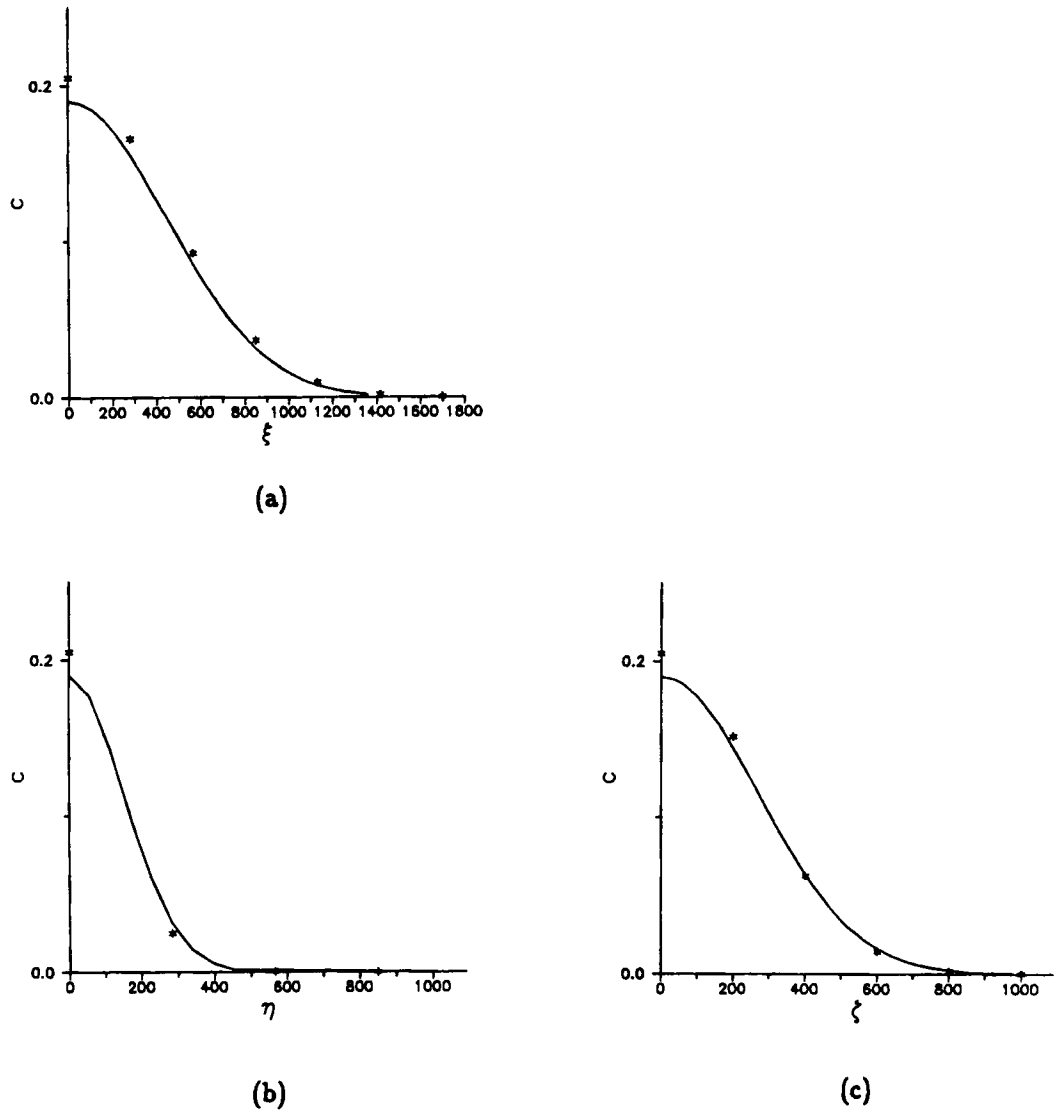

Figure 10. Result of second advection–diffusion example in local co-ordinates (a) ξ, (b) η and (c) ζ: ——, analytical; *, TLS

5. DISCUSSION

The accuracy of the TLS scheme has been shown for the one- and two-dimensional advection–diffusion equation in our previous study.[1] In this study the TLS scheme is applied to the three-dimensional advection–diffusion equation to demonstrate its accuracy using some numerical examples of severe conditions. The serendipity Hermite element is selected as the shape function on a linear hexahedral element. The serendipity function has derivative unknowns in local co-ordinates, which proves to be advantageous in handling derivative boundary conditions without integration by parts.

The 3D TLS scheme is tested against the 2D example used in the previous study for the purpose of, in part, validation of the code and, in part, sensitivity analysis of the scheme on the different

types of shape functions. In 2D a special non-conforming Hermite shape function on a triangle[9] is used. Compared to the 2% dissipation of the 2D result, the TLS has about 5% dissipation at the peak, indicating that the scheme is rather sensitive to the types of shape functions.

Four 3D examples are reported in this study. The first two are advection of a steep Gaussian hill and the other two are advection–diffusion of a cloud diffused from a point source. For the advection problems the steep 3D Gaussian hill is placed in rotating flow fields: one with zero rate of strain and the other with non-zero rate of strain. About 10%–14% dissipation at the peaks is observed. Considering the severity of the initial condition and the flow field, the results are very good. Moreover, the spherical symmetry is well preserved, which indicates excellent phase accuracy of the Taylor–least squares scheme. For the advection–diffusion example the initial conditions are obtained by diffusing a point source subject to the constant diffusion tensors and predetermined flow field. Then the ray method is used to determine the analytical solutions as initial conditions for the examples, which are even steeper than those of the advection examples. The hill is contained in just two elements in that its value is less than 1% of the peak two elements away from the centre. The diffusion coefficients are selected such that the grid Peclet numbers range from 10 to 90, indicating that the transport is advection-dominated. Deviations of the TLS results compared to the analytical solutions are about 8% at the peak in both cases. The error compares favourably to that of the advection examples owing to the presence of the well-behaved diffusion part. However, it is important to recognize that the initial conditions are steeper than those of the advection problems. Therefore direct comparison of the error rates would be unfair.

The three-dimensional Taylor–least squares finite element method can solve both pure advection and advection–diffusion problems well. The scheme provides a viable tool for the difficult class of advection-dominated problems.

ACKNOWLEDGEMENTS

This work was supported in part by a grant from the National Science Foundation (ECE-8610119) and conducted using the Cornell National Supercomputer Facility, a resource of the Center for Theory and Simulation in Science and Engineering (Theory Center), which receives major funding from the National Science Foundation and IBM Corporation with additional support from New York State and members of the Corporate Research Institute. The authors also wish to thank Dr. Sudicky for his conjugate gradient solver and HydroGeoLogic, Inc. for its computing resources.

REFERENCES

1. N.-S. Park and J. A. Liggett, 'Taylor–least squares finite element for two-dimensional advection-dominated advection–diffusion problems', *Int. j. numer. methods fluids*, **11**, 21–38 (1990).
2. J. Donea, L. Quartapelle and V. Selmin, 'An analysis of time discretization in the finite element solution of hyperbolic problems', *J. Comput. Phys.*, **70**, 463–499 (1987).
3. G. F. Carey and B. N. Jiang, 'Least-squares finite elements for first-order hyperbolic systems', *Int. j. numer. methods eng.*, **26**, 81–93 (1988).
4. L. Lapidus and G. F. Pinder, *Numerical Solutions of Partial Differential Equations in Science and Engineering*, Wiley–Interscience, New York, 1982.
5. A. M. Baptista, 'Reference problems for the convection–diffusion forum', *Proc. VIth Int. Conf. on Finite Elements in Water Resources*, Lisbon, Portugal, 1986.
6. J. K. Cohen and R. M. Lewis, 'A ray method for the asymptotic solution of the diffusion equation', *J. Inst. Math. Appl.*, **3**, 266–290 (1967).
7. R. Smith, 'The early stages of contaminant dispersion in shear flows', *J. Fluid Mech.*, **111**, 107–122 (1981).
8. A. D. Taylor, 'Solutions of diffusion–advection problems by ray methods', unpublished (see Reference 7).
9. G. Bazeley, Y. Cheung, B. Irons and O. C. Zienkiewicz, 'Triangular elements in plate bending—conforming and nonconforming solutions', *Proc. (First) Conf. on Matrix Methods in Structural Mechanics, AFFDL TR 66–80*, 1965, pp. 547–576.